MICROROBOTS

Gastrointestinal tract drug delivery using algae motors embedded in a degradable capsule

Fangyu Zhang†, Zhengxing Li†, Yaou Duan†, Amal Abbas, Rodolfo Mundaca-Uribe, Lu Yin, Hao Luan, Weiwei Gao, Ronnie H. Fang, Liangfang Zhang*, Joseph Wang*

The use of micromotors for active drug delivery via oral administration has recently gained considerable interest. However, efficient motor-assisted delivery into the gastrointestinal (GI) tract remains challenging, owing to the short propulsion lifetime of currently used micromotor platforms. Here, we report on an efficient algae-based motor platform, which takes advantage of the fast and long-lasting swimming behavior of natural microalgae in intestinal fluid to prolong local retention within the GI tract. Fluorescent dye or cell membrane–coated nanoparticle functionalized algae motors were further embedded inside a pH-sensitive capsule to enhance delivery to the small intestines. In vitro, the algae motors displayed a constant motion behavior in simulated intestinal fluid after 12 hours of continuous operation. When orally administered in vivo into mice, the algae motors substantially improved GI distribution of the dye payload compared with traditional magnesium-based micromotors, which are limited by short propulsion lifetimes, and they also enhanced retention of a model chemotherapeutic payload in the GI tract compared with a passive nanoparticle formulation. Overall, combining the efficient motion and extended lifetime of natural algae–based motors with the protective capabilities of oral capsules results in a promising micromotor platform capable of achieving greatly improved cargo delivery in GI tissue for practical biomedical applications.

INTRODUCTION

Oral delivery to the gastrointestinal (GI) tract has been one of the most widely used approaches for drug administration due to its high patient compliance, noninvasiveness, simplicity, and low cost (*1*, *2*). Despite their potential advantages, oral drug formulations face several barriers within the GI tract, including poor stability in gastric fluid, limited drug interaction with the intestinal lining, and low solubility (*3*). Several engineered systems, based on microinjectors and microneedles, have been described recently for improving the oral delivery of large biological macromolecules via mechanical penetration mechanisms (*4*, *5*). Other platforms, including bioadhesive patches, responsive hydrogels, mucus-penetrating particles, ionic liquids, and microgrippers, have been reported for enhancing GI delivery via improved tissue adhesion, prolonged retention, and improved drug localization (*6*–*10*). The use of micromotors is another promising and effective approach for the active transport of therapeutic agents to specific sites of interest (*1*, *11*–*14*). A variety of synthetic micromotors, capable of propelling to hard-to-reach locations within the body, have been developed for active drug delivery and for other biomedical applications, including biosensing and microsurgery (*15*–*19*). Early in vivo studies using micromotors focused primarily on the GI tract, which can provide a favorable environment for movement (*19*, *20*). These pioneering studies used chemically powered micromotors based on magnesium (Mg) or zinc microengines for the enhanced delivery of antibiotics, vaccines, and micronutrients (*19*–*22*). These self-propelled micromotors hold particular promise for the local delivery of drug payloads toward the treatment of GI diseases and disorders (*19*). Although these active platforms substantially enhanced delivery efficacy compared with corresponding static microcarriers, they suffer from short lifetimes of operation up to about 15 min once in contact with GI fluid. This decreases the potential of these synthetic micromotors to interact with GI mucosa and limits their overall retention, thus leading to decreased drug bioavailability. To address this limitation, active micromotor-based GI drug delivery systems with improved characteristics need to be developed.

Here, we report an algae motor–loaded capsule system that combines the efficient long-lasting movement of natural algae in the small intestine with the protective capabilities of oral capsules, thus enabling prolonged retention within the intestinal mucosa toward greatly improved GI delivery (Movie 1). Microorganisms such as bacteria, sperm, and microalgae have evolved over millions of years to develop robust actuation systems that enable autonomous motion (*23*). These natural cellular systems have recently emerged as attractive cargo carriers that are capable of transporting

Movie 1. Algae biohybrid micromotor-loaded oral capsule for GI drug delivery.

Department of NanoEngineering and Chemical Engineering Program, University of California San Diego, La Jolla, CA 92093, USA.
*Corresponding author. Email: josephwang@ucsd.edu (J.W.); zhang@ucsd.edu (L.Z.)
†These authors contributed equally to this work.

therapeutics to hard-to-reach body locations (*24*, *25*). Combining these motile microorganisms with synthetic materials results in biohybrid systems capable of performing multiple tasks (*26*–*28*). Whereas sperm and bacteria have been used for over a decade in diverse biomedical applications ranging from cancer therapy to assisted fertilization (*29*–*31*), microalgae swimmers have rarely been explored as robotic actuators (*32*). Microalgae are eukaryotic swimmers that are facile to culture, and they offer attractive properties for biomedical applications, including efficient propulsion (>100 μm/s), autofluorescence, and phototactic guidance capabilities.

We chose *Chlamydomonas reinhardtii* as a model microalgal swimmer for active payload delivery in the GI tract because of its many attractive properties, including cytocompatibility, cost-effective scalable production, good adaptability and motility in diverse aqueous environments, abundance of reactive surface groups for functionalization, and autofluorescence for ease of tracking in vivo (*27*, *32*–*34*). *C. reinhardtii* swims by beating its two flagella synchronously at a frequency of 50 Hz (*35*), reaching high speeds up to about 200 μm/s (*32*, *36*). We demonstrate that *C. reinhardtii* display substantially longer propulsion in intestinal fluid compared with synthetic chemically powered Mg micromotors, which are the only type of self-propelled microrobot swimmers that have been reported for in vivo operation in the GI tract (*19*–*22*). To protect the algae motors from the harsh gastric environment, we embedded them inside a protective capsule (Fig. 1, A to C), which was prepared with an inner hydrophobic coating to entrap aqueous solution for maintaining algae viability along with an outer pH-responsive enteric polymer coating. Upon release from the capsule, the algae display constant motility in intestinal fluid (Fig. 1D). Compared with the short lifetime of commonly used Mg micromotors, the algae motors remain motile for more than 12 hours at body temperature. In vivo, this prolonged movement leads to notably improved intestinal distribution (Fig. 1E), resulting in enhanced retention of a model chemotherapeutic doxorubicin (Dox) conjugated to the algae motors. Overall, our findings indicate that natural algae–based active carriers hold great promise for oral drug delivery to enhance the treatment of GI diseases.

RESULTS

Movement of algae-based micromotors in simulated intestinal fluid

We first studied the motion properties of *C. reinhardtii*, which are commonly used as a model algal species (*37*), and compared them with those of Mg micromotors (Fig. 2A). Simulated intestinal fluid (SIF), mainly composed of potassium dihydrogen phosphate at pH 6.8, was used to test the movement of the algae and Mg micromotors. In SIF, the natural algae motors exhibited a stable speed profile of about 120 μm/s that lasted for a minimum of 12 hours (movie S1). This consistent motile behavior is ascribed to the coordinated, self-sustained beating of algae flagella (*38*) even under suboptimal survival conditions, such as SIF. In contrast, the speed of Mg micromotors in SIF markedly decreased from an initial 180 to 80 μm/s after 15 min before reaching 0 μm/s after another 15 min (movie S2). This sharp drop in speed reflects the rapid dissolution and depletion of the Mg engine during propulsion. The percentage of motile Mg motors also dropped to 20% after 15 min of propulsion, whereas 89% of the algae motors remained moving after 12 hours (Fig. 2B). In tracing their motion, the movement patterns of algae tracked over 2-s intervals appeared consistent over the course of 12 hours (Fig. 2C and movie S3), whereas no movement was observed for Mg motors after 30 min (Fig. 2D and movie S4). These data illustrated that the algae motors could self-propel efficiently in SIF and maintain consistently fast motility over long periods of time, thereby supporting their potential for active GI delivery applications.

To demonstrate their potential for drug delivery, we modified the algae motors with two different cargos: a fluorescent dye and polymeric nanoparticles (NPs). The green dye fluorescein (excitation/emission = 494 nm/518 nm) was first chemically conjugated to the surface of the algae (*39*). After dye conjugation, the algae could be fluorescently tracked (Fig. 2, G and H, and movie S5), and the median speed calculated from 100 individual algae was nearly identical to that of unmodified algae (Fig. 2, E and F, and movie S5) and consistent with previously reported values (*32*, *36*). Similarly, red blood cell (RBC) membrane–coated poly(lactic-*co*-glycolic acid) (PLGA) NPs (*40*) were linked to the algae via click chemistry. To visualize the NPs on the algae, we encapsulated the fluorescent dye 1,1′-dioctadecyl-3,3,3′,3′-tetramethylindocarbocyanine (DiI; excitation/emission = 550 nm/567 nm) inside the PLGA core during the fabrication process. The NP-modified algae motors (denoted "algae-NP motors") exhibited a similar swimming pattern and speed distribution profile in SIF compared with unmodified algae motors (Fig. 2, I and J, and movie S5). In addition, the intrinsic phototaxis of the algae was not compromised after the NP functionalization (movie S6). The data here confirmed that different payloads, ranging from small molecules to NPs, can be successfully loaded onto algae motors without affecting their propulsion characteristics, further highlighting the active GI delivery potential of algae-based motor systems.

Formulation of algae motors into protective capsules

To effectively use algae motors for delivery to the GI tract in vivo, it is necessary to overcome the harsh acidic environment of the stomach, which can degrade the algae before they reach the small intestines. To address this, we modified a commercial capsule to encapsulate viable algae in an internal aqueous medium for safe passage through the stomach. First, an organosilicon solution, consisting of 4% octadecyltrimethoxysilane (OTMS) (*41*), was prepared to create a thin hydrophobic coating on the inside of the capsule via a thermal evaporation technique (fig. S1A). To test the stability of a capsule with this internal coating, we encapsulated an aqueous solution containing rhodamine dye. Visually, the capsule remained unchanged, whereas notable deformation was observed for a control uncoated capsule (fig. S1, B and C). By changing the number of coating layers, we could modulate the degradation of the capsules, which is reflected by the release of the dye, with 10 layers of coating offering the longest delay in release in SIF (fig. S1, D and E). Second, the exterior surface of the capsule was coated with Eudragit L100-55, a pH-responsive polymer commonly used for protecting oral medication from harsh gastric acid conditions (fig. S2A); previous studies have demonstrated the utility of Eudragit L100-55 as an enteric coating for enhancing the delivery of micromotors to the intestines (*42*). To imitate physiological conditions in the stomach, we used simulated gastric fluid (SGF) at pH 1.5, containing sodium chloride and hydrochloric acid. In our case, three layers of coating using a 7% (w/v) polymer solution offered full protection of the encapsulated cargo from SGF (fig. S2B).

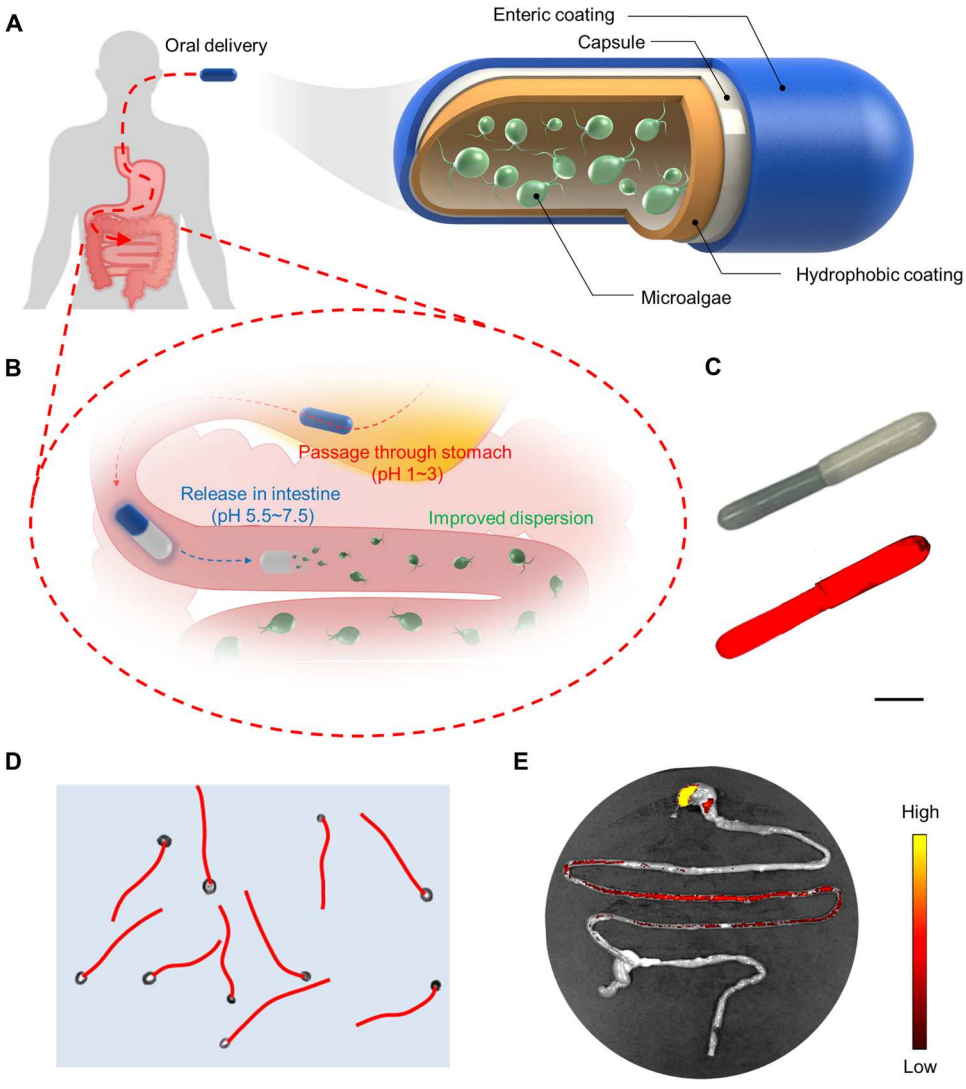

Fig. 1. Schematic of algae motors in a capsule for GI tract delivery. (**A**) Algae motors loaded within protective capsules containing an inner hydrophobic coating layer and an outer enteric coating layer can be used for oral delivery applications. (**B**) The algae motor–loaded capsule first enters the stomach, where the enteric coating protects it from degradation at acidic gastric pH. Upon entering the intestines, the enteric coating is dissolved in the nearly neutral pH and the capsule is degraded, leading to complete release of the algae motors. (**C**) Bright-field (top) and fluorescent (bottom) images of an algae motor-loaded capsule. Scale bar, 2 mm. (**D**) Representative tracking trajectories demonstrating the autonomous movement of algae motors in simulated intestinal fluid. (**E**) Representative biodistribution of fluorescently labeled algae motors in the GI tract 5 hours after administration in a capsule by oral gavage.

Upon changing from SGF to SIF, burst cargo release was observed within 10 min because of dissolution of the enteric coating at higher pH values (fig. S2C). These results confirmed that it was possible to load cargo in aqueous solutions using suitably coated capsules for the GI delivery of algae motors.

Next, we investigated the encapsulation of live algae into the modified capsules and their release in vitro. Algae were suspended in tris-acetate-phosphate (TAP) medium and loaded into capsules with 10 inner OTMS layers and 3 outer enteric coating layers. For visualization, the OTMS and enteric coating layers were labeled with 3′,3′-dioctadecyloxacarbocyanine (DiO; excitation/emission = 484 nm/501 nm) and Pacific Blue (excitation/emission = 410 nm/455 nm), respectively. Under fluorescence microscopy, a strong signal was observed for both coating layers along with the autofluorescence of the algae (excitation/emission = 647 nm/680 nm), confirming the successful encapsulation of algae motors into the fabricated capsule platform (Fig. 3A). In SGF, it was demonstrated that there was no release of algae from the capsules, whereas the algae motors could be released over time in SIF (Fig. 3B). The release in SIF was gradual for about 30 min, after which most of the algae was released by 45 min from the start of the experiment. The total number of released algae reached 9.15×10^5 after 45 min (Fig. 3, C and D). Motion tracking of algae motors within the capsule and algae motors released from the capsule revealed similar patterns of movement (Fig. 3E and movie S7). The median speed calculated from 100 individual algae also remained unchanged throughout the fabrication process and after release from the capsules (Fig. 3, F and G, and

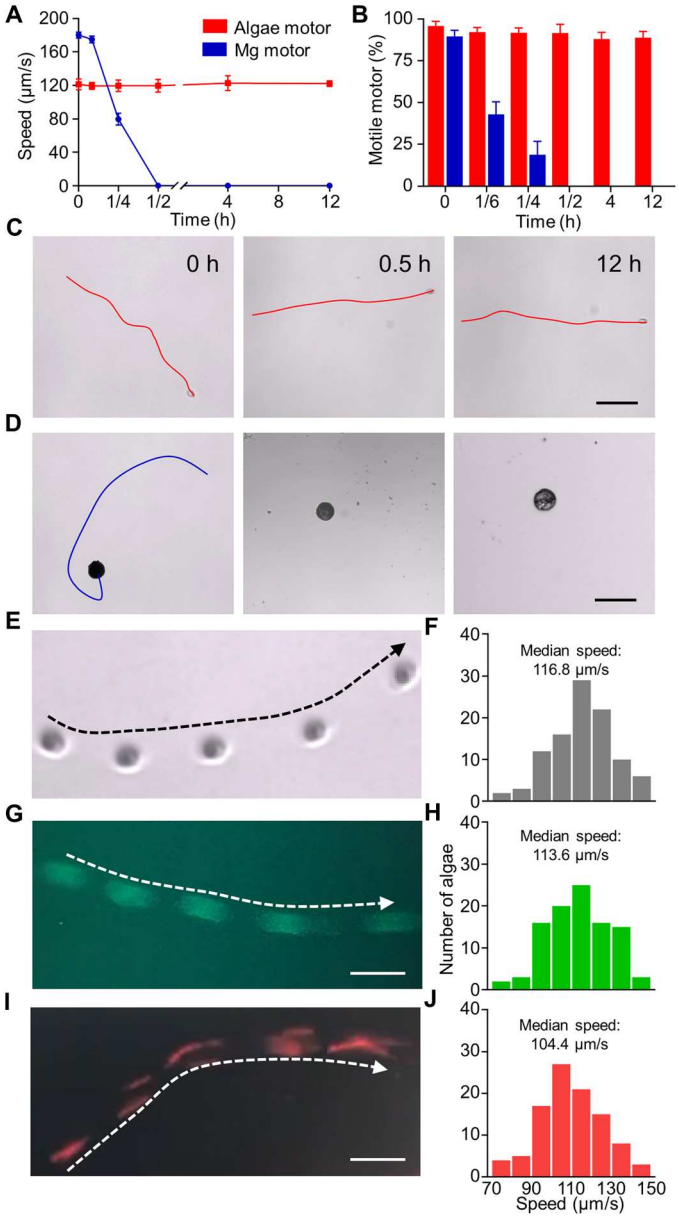

Fig. 2. Motility of algae motors and Mg motors in SIF at room temperature. (**A**) Speed of algae motors and Mg motors in SIF during 12 hours of operation (n = 5, means ± SD). (**B**) The percentage of motile motors in SIF during a 12-hour period (n = 5, means + SD). (**C** and **D**) Time-lapse snapshots and trajectories of algae motors (C) and Mg motors (D) over a span of 2 s at different time points during operation. Scale bars, 50 μm. (**E** to **J**) Time-lapse images showing trajectories over a span of 1 s and corresponding speed distributions of unmodified algae (E and F), fluorescein-labeled algae motors (G and H), and algae motors carrying DiI-loaded RBC membrane–coated NPs (I and J) (n = 100). Scale bars, 20 μm.

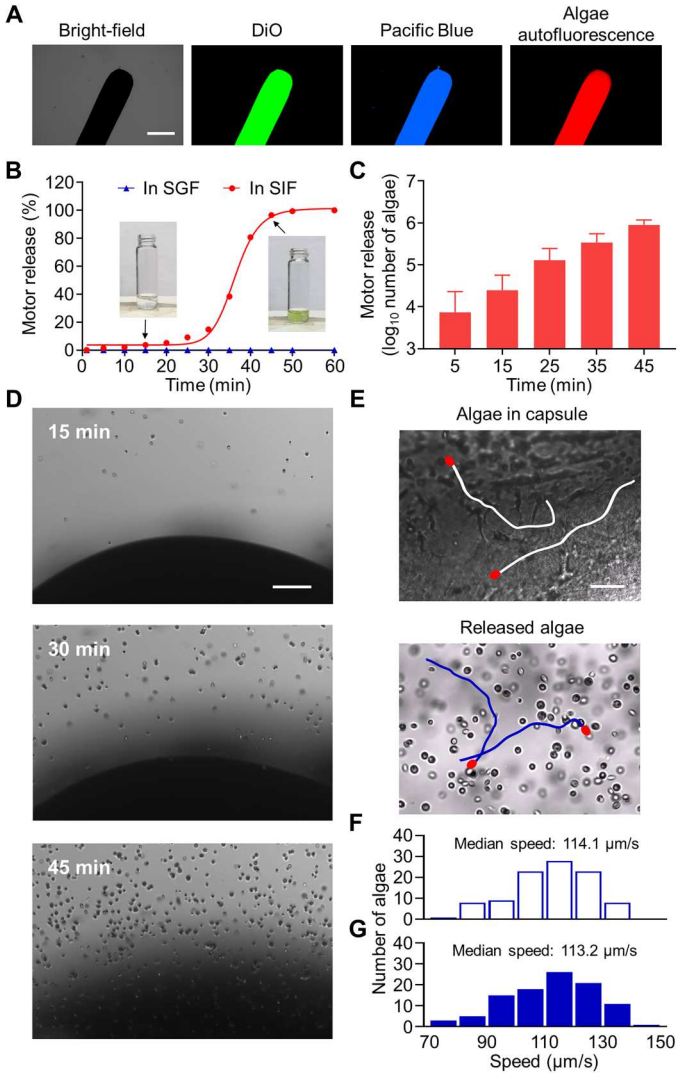

Fig. 3. Loading and release of algae motors in a capsule in vitro. (**A**) Bright-field and fluorescence microscopy images of autofluorescence of algae motors (red) in a capsule formulation fabricated with a DiO-labeled OTMS inner coating (green) and a Pacific Blue–labeled enteric outer coating (blue). Scale bar, 1 mm. (**B**) Release profile of algae motors from a capsule in SGF (blue line) and SIF (red line). Inset images correspond to t = 15 min (left) and t = 45 min (right). (**C**) Quantification of algae release from capsules over time in SIF (n = 3, means + SD). (**D**) Time-lapse images (t = 15, 30, and 45 min) showing the release of algae motors from a capsule in SIF. Scale bar, 100 μm. (**E**) Representative tracking lines (captured from movie S7) of encapsulated algae motors in TAP medium and released algae motors in SIF. Scale bar, 50 μm. (**F** and **G**) Speed distribution of the encapsulated algae motors (F) and released algae motors (G) from (E) (n = 100).

fig. S3). These data indicated that the algae motors could be effectively encapsulated and then released from the modified capsule with negligible effect on their swimming performance.

After evaluating the release of algae motors from the capsules under in vitro conditions, we investigated the delivery capabilities of the platform within the GI tract. First, mimicking the physiological conditions of the intestines, the motion behavior of algae motors and Mg motors was evaluated in SIF at 37°C in vitro (Fig. 4, A and B). The speed of the algae motors was affected by the elevated temperature (movie S8), decreasing from 113 to 83 μm/s within 15 min of self-propulsion and further dropping to 40 μm/s after 12 hours. At the experimental endpoint, about 70% of the algae remained motile, indicating that they could survive for prolonged periods of time even under unfavorable conditions. In comparison, the conventional Mg motors rapidly lost their movement (movie S9), with only 33% still propelling at a high speed of 180 μm/

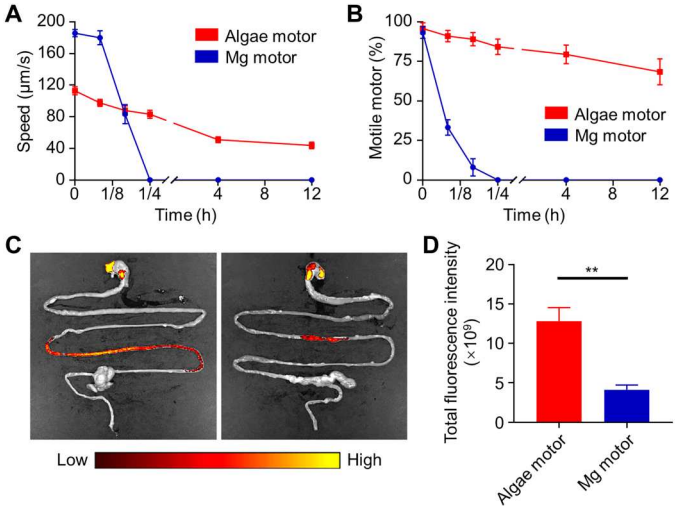

Fig. 4. Comparison of the distribution of algae motors and Mg motors in the GI tract. (**A**) Speed of algae motors and Mg motors at 37°C in SIF during 12 hours of operation (n = 5, means ± SD). (**B**) Percentage of motile algae motors and Mg motors at 37°C in SIF during 12 hours of operation (n = 5, means ± SD). (**C**) Representative images of the GI tracts of mice 5 hours after oral administration of fluorescein-labeled algae motors in a capsule (left) or Mg motors in a capsule (right). (**D**) Quantitative analysis of total fluorescence intensity within the small intestine from the images in (C) (n = 3, means + SD). Student's two-tailed t test, $^{**}P < 0.01$.

s after 5 min. After another 10 min, only 8% remained motile, with an average speed of 80 μm/s. This fast drop in speed and the fraction of motors displaying active motion reflected the rapid depletion of the Mg engine. The algae motors also exhibited the ability to swim in viscous simulated mucus (*43*) over an extended period of time, whereas the Mg motors did not (fig. S4). These findings illustrated the greatly improved behavior of the algae motors compared with their Mg-based counterparts for potential GI applications requiring prolonged propulsion.

In vivo biodistribution of algae motors after oral delivery

After the in vitro tests, a study was carried out to assess the in vivo biodistribution and retention of the algae motors when delivered orally in capsule form. To facilitate imaging and quantification in biological tissue, we labeled the algae motors and Mg motors with the same fluorescent dye (fig. S5). The algae motors were directly conjugated with fluorescein, whereas the Mg motors were first coated with poly-L-lysine (*44*), then conjugated with the dye. As a result, both motors could be easily visualized under fluorescence microscopy and displayed near-identical signals that did not diminish after 6 hours in SIF at 37°C. Next, the algae motors and Mg motors were embedded in the protective capsules and administered by oral gavage to mice. At 5 hours after administration, the mice were euthanized, and their GI tracts were imaged ex vivo (Fig. 4C). Whereas a narrow distribution was observed from the fluorescent signal of the Mg motors, the signal for the algae motors was more broadly distributed through the intestines (fig. S6). Quantification of the total radiant efficiency within the small intestines corroborated the improved retention of the algae motors compared with the Mg motors (Fig. 4D). The observed differences in biodistribution suggested that algae, with their long-lasting movement properties, could be effective at delivering drug payloads locally within the GI tract.

In vivo delivery of therapeutic drugs using algae motor capsules

To better understand the mechanism behind the improved biodistribution and retention of algae motors within the small intestine, we compared our algae motor capsule formulation with different control groups, including TAP medium only (negative control), free algae without a capsule, and static algae in a capsule. To

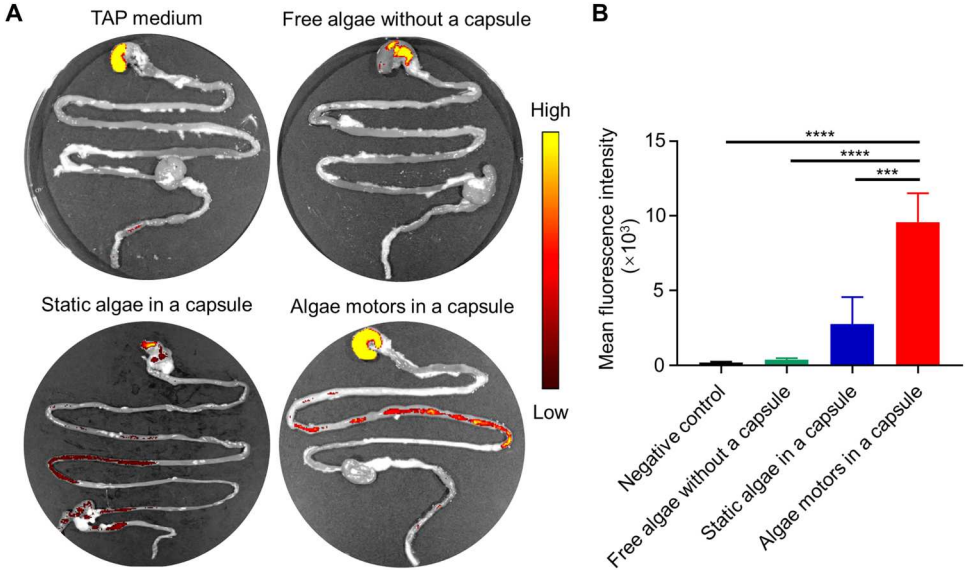

Fig. 5. GI tract delivery of algae motors in comparison with other algae controls. (**A**) Representative ex vivo fluorescence images of GI tissues of mice 5 hours after oral administration with TAP medium as a negative control, free algae without a capsule, static algae in a capsule, and algae motors in a capsule. (**B**) Quantitative analysis of the mean fluorescence from the experiment in (A) (n = 3, means + SD). One-way ANOVA, $^{***}P < 0.001$ and $^{****}P < 0.0001$.

prepare the static algae control, we deflagellated live algae using acetic acid and resuspended them in phosphate-buffered saline (PBS) for encapsulation. Optical visualization and scanning electron microscopy (SEM) images confirmed successful deflagellation and that the resulting static algae lost their motion capabilities in SIF at 37°C (fig. S7 and movie S10). The intrinsic fluorescence of chlorophyll *a* in algal chloroplasts allows for noninvasive fluorescence imaging of algae without the need for chemical modification (*45*). We then proceeded to perform ex vivo fluorescence imaging on the GI tracts of mice receiving the various formulations with equivalent fluorescence to determine the influence of active movement and capsule protection on biodistribution (Fig. 5A and fig. S8). At 5 hours after oral administration, algae motors delivered inside capsules were more broadly distributed across the intestines compared with static algae that were also encapsulated. This result highlighted the importance of self-propulsion, which likely helped to increase the interaction of the algae with the intestinal wall, thus leading to enhanced retention. In addition, there was almost no signal observed in the intestines after administration of free algae, demonstrating the necessity of using the capsules to protect from the harsh stomach acid. Quantification of the fluorescent signal from each sample further supported the imaging results, as the fluorescence from the encapsulated algae motor group was 3.5-fold greater than that of the encapsulated static algae group (Fig. 5B). To control for the background signal from food contaminants within the stomach (*42*, *46*), we delivered capsules containing algae motors labeled with Cyanine7 (Cy7; excitation/emission = 750 nm/773 nm) orally, and it was confirmed that most of the algae were distributed within the intestine (fig. S9).

We next explored the feasibility of using algae motors for delivering therapeutic drugs to the GI tract. Dox, a commonly used frontline chemotherapeutic agent (*47*), was selected as a model drug payload. First, RBC membrane–coated NPs were loaded with Dox [denoted "NP(Dox)"] via a double emulsion solvent evaporation technique (*48*, *49*). Transmission electron microscopy (TEM) imaging confirmed the core-shell structure of the NPs (fig. S10). Fluorescence imaging showed colocalization of the Dox-loaded PLGA cores and the DiO-labeled RBC membrane coating, verifying successful drug loading (fig. S11). Next, NP(Dox) was linked to the algae [denoted "algae-NP(Dox)"] by click chemistry (Fig. 6A). Fluorescence and SEM imaging confirmed the effective binding of NP(Dox) to the algae (Fig. 6, B and C). To test the Dox loading onto the algae, we incubated 1×10^6 algae with different concentrations of NP(Dox). The Dox loading yield onto the algae was measured at different NP(Dox) inputs, and the maximum loading amount (15 μg) was obtained with a 50-μg input of Dox, corresponding to a 30% loading efficiency per 10^6 cells (Fig. 6D). It was also confirmed that Dox, either in free form or nanoparticulate form, did not influence the viability of the algae (fig. S12). The mean and median speed of algae-NP(Dox) measured from 100 individual algae motors were 108.69 and 108.78 μm/s, respectively, and these values were comparable with those of the bare algae (Fig. 6, E and F). Furthermore, it was demonstrated that the drug release profile of NP(Dox) was not affected by binding to the algae motors (Fig. 6G). After loading onto algae motors, the NP(Dox) payload retained its cytotoxic activity, as it was demonstrated that algae-NP(Dox) could inhibit the growth of B16F10 melanoma cell lines in vitro (Fig. 6H). Algae-NP(Dox) and NP(Dox), both loaded into protective capsules, were then administered at the same drug dosage, followed by extraction of the intestines to quantify Dox concentration (Fig. 6I). Compared with the tissue homogenates of mice administered with NP(Dox), the samples from mice receiving algae-NP(Dox) exhibited significantly higher drug levels at all of the time points (3, 6, and 9 hours) that were tested. These data further supported the benefits of using algae motors with prolonged active self-propulsion to enhance the delivery and retention of therapeutic payloads in the small intestinal tissues. Future studies will focus on evaluating the potential of algae motors for drug delivery to treat diseases in suitable animal models, such as for inflammatory bowel disease and bacterial gastroenteritis.

In vivo toxicity evaluation of algae motor capsules

Last, we evaluated the in vivo safety profile of the algae motor capsule platform after oral administration. A comprehensive blood chemistry panel and blood cell count were conducted 24 hours after administration (Fig. 7, A and B). Compared with untreated control mice, the levels of all serum biochemistry markers and numbers of blood cells (RBCs, white blood cells, and platelets) in the mice receiving algae motor capsule treatment remained at normal levels. A longer-term safety study in which mice were administered with one algae motor capsule on days 0, 2, 4, and 6 also yielded the same result, whereby negligible toxicity, indicated by the minor changes in metabolic biomarkers and blood cell counts, to the mice was observed. Histological analysis of GI tract tissue sections from algae motor-treated mice stained with hematoxylin and eosin (H&E) revealed that structural integrity was preserved and that there was no immune cell infiltration into the mucosa or submucosa, indicating the lack of an inflammatory response (Fig. 7C). There was also no observable inflammation or pathological changes on H&E-stained sections from other major organs such as the heart, lungs, liver, kidneys, and spleen (Fig. 7D). Overall, these results suggested that the algae motor capsule platform is safe to use for oral drug administration.

DISCUSSION

The development of microorganism-based micromotors for addressing key health care issues is still in its infancy (*25*). Although various in vitro studies have illustrated the use of bacteria-based drug delivery systems, there are major risks associated with their in vivo use when considering factors such as pathogenicity or immunogenicity (*24*). As an alternative cell type, microalgae are nonpathogenic and have been explored in the development of biohybrid systems (*36*, *50*). Microalgal swimmers recently have been used as biomedical robotic actuators, primarily under in vitro settings (*32*). Early in vivo studies have mainly focused on the therapeutic delivery of algae-derived compounds (*51*). More recently, a few studies have reported the use of algae as drug carriers for in vivo operation (*45*, *52*). For example, the spiral structure of *Spirulina platensis* was leveraged to passively prolong retention of curcumin in the intestines for the improved treatment of colon cancer and colitis (*45*). In addition, a magnetic NP-loaded microalgae biohybrid imaging system was reported recently, and a swarm of these microswimmers could be externally controlled by a magnetic field and tracked using magnetic resonance imaging (*50*). Despite these advances, there have been no studies exploiting the intrinsic self-propulsion of algae for enhanced GI delivery.

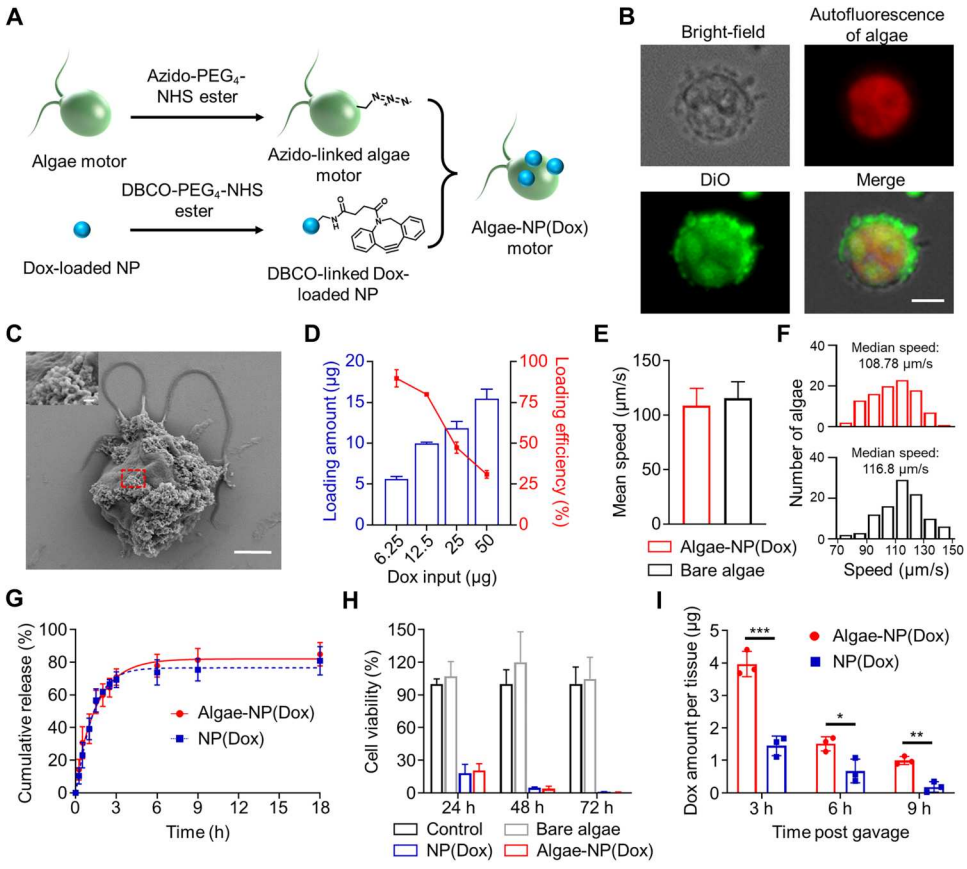

Fig. 6. Characterization of drug-loaded algae motors. (**A**) Schematic illustration of the fabrication process for the algae-NP(Dox) motor. (**B**) Bright-field and fluorescence microscopy images visualizing the autofluorescence of algae chloroplasts (red) and DiO-labeled RBC membrane (green) to demonstrate the loading of Dox-loaded NPs onto an algae motor. Scale bar, 5 μm. (**C**) SEM image of an algae motor loaded with NP(Dox). Scale bar, 2.5 μm. Inset shows a zoomed-in view corresponding to the dashed red box. Scale bar, 200 nm. (**D**) Quantification of drug loading amount and loading efficiency of 1×10^6 algae-NP(Dox) at different Dox inputs ($n = 3$, means ± SD). (**E** and **F**) Mean (E) and median (F) speed of algae-NP(Dox) motor and bare algae. The speed was measured from 100 individual alga. (**G**) The cumulative drug release profiles from the algae-NP(Dox) motor and NP(Dox) ($n = 3$, means ± SD). (**H**) Viability of B16-F10 cancer cell lines after 24, 48, and 72 hours of incubation with blank solution, bare algae, NP(Dox), and algae-NP(Dox) motor ($n = 3$, means ± SD). (**I**) Quantification of the total Dox content per small intestine at different times after administration of the algae-NP(Dox) motor and NP(Dox) in a capsule ($n = 3$, means ± SD). Student's multiple *t* test, $^*P < 0.05$, $^{**}P < 0.01$, and $^{***}P < 0.001$.

In the present study, several key points have been considered to tackle the challenges facing algae-based active GI delivery: protection from the harsh acidic environment of the stomach en route to the intestines, selection of a suitable algal strain with long-lasting self-propulsion in intestinal fluid, and cargo/drug loading capability. By addressing these issues, we demonstrated here an algae motor capsule system for effective intestinal targeting and prolonged tissue retention. Compared with the short lifetime of current Mg-based micromotors, the algae motors displayed prolonged propulsion in GI fluid toward enhanced local delivery for the treatment of potential GI diseases and disorders. To achieve intestinal delivery, we fabricated an enteric-coated capsule modified with an inner hydrophobic organosilicon layer to effectively protect encapsulated algae from the harsh gastric fluid while maintaining their viability. The capsule fabrication, encapsulation, and release processes had a negligible effect on the viability of the algae motors. Modifying capsules in the manner described here provides an effective approach for delivering motile living organisms in aqueous media to the GI tract. To demonstrate the distinct advantages of the platform for in vivo intestinal delivery, we administered algae motor capsules orally, and their biodistribution and retention properties were compared with various controls. The algae motors displayed broader distribution and stronger retention in the GI tract compared with synthetic Mg motors. This was likely mediated by the prolonged motion of the live algae, because it was shown that static algae that were incapable of propulsion exhibited considerably less retention in the intestines. We also demonstrated that the ability of the algae motor capsule system could also be used for the delivery of a model anticancer drug to the GI tract. Moreover, the platform displayed a favorable biosafety profile after oral administration.

The characteristics of the algae motor in a capsule formulation, particularly its long-lasting self-propulsion, can be leveraged for microrobotic biomedical applications beyond the treatment of GI diseases and disorders, ranging from GI detoxication to imaging and sensing. There are several approaches in which algae motors could be improved to enhance their utility for GI delivery applications. For example, the incorporation of imaging agents could enable direct visualization of algae movement as they operate within the intestines. A recent report described a photoacoustic computed tomography–guided microrobotic system for realizing real-time

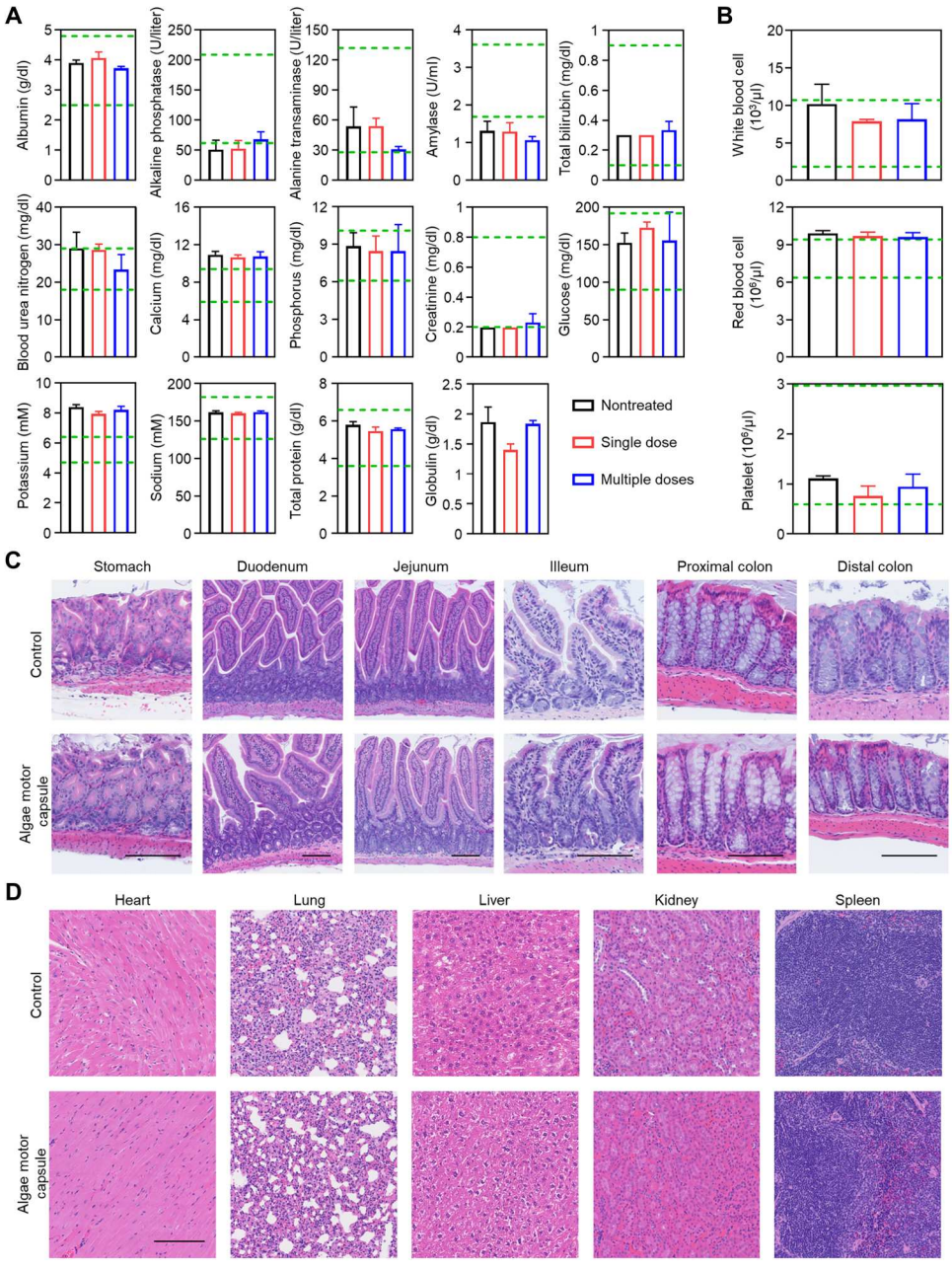

Fig. 7. In vivo safety analysis of algae motors after oral administration. (**A** and **B**) Comprehensive blood chemistry panel (A) and blood cell counts (B) taken from nontreated mice, mice with single-dose treatment, and mice with multiple-dose treatment ($n = 3$, means + SD). For single-dose evaluation, mice were orally administered with one algae motor capsule on day 0, and blood samples were collected on day 1. For multiple-dose evaluation, mice were orally administered with one algae motor capsule on days 0, 2, 4, and 6. Blood samples were collected on day 7. The green dashed lines indicate the mouse reference ranges of each analyte. (**C**) Representative H&E-stained histological sections from different sections of the GI tract from nontreated mice and mice treated with the algae motors in a capsule 24 hours after oral administration. Scale bars, 100 μm. (**D**) H&E-stained histological sections of major organs, including the heart, lungs, liver, kidneys, and spleen, from nontreated mice and mice treated with the algae motors in a capsule 24 hours after oral administration. Scale bar, 250 μm.

navigation and monitoring of synthetic Mg motors in the intestines in vivo (*53*). In another example, positron emission tomography combined with computed tomography was used to evaluate the swarm behavior of enzyme-powered nanomotors in the bladder (*17*). By conjugating magnetic microparticles to the algae surface (*32*), an external magnetic navigation system could be used to precisely guide and track algae motors to target sites. Whereas the current work focused on demonstrating the potential of algae motor capsules for enhancing intestinal delivery, future work will be required to confirm the therapeutic advantages of the platform in clinically relevant disease models, such as those for bacterial GI infection, irritable bowel disease, or colon cancer. Microalgae can also be engineered to express biologic payloads that can be produced in situ after oral administration (*54*, *55*). The properties of

the capsules can be tuned to more precisely target specific regions of the GI tract (*42*). Overall, functionalized algae motors, loaded within a protective capsule, represent an attractive biohybrid motor system that can be applied across a wide range of biomedical applications.

MATERIALS AND METHODS

Algae culture

The green algae *C. reinhardtii* (strain CC-125 wild-type mt+) were obtained from the *Chlamydomonas* Resource Center. The algae were transferred from the agar plate to TAP medium (Thermo Fisher Scientific) and cultured at room temperature under cycles of 12-hour sunlight and 12-hour dark.

Preparation of Mg micromotors

Mg micromotors were fabricated using 20 ± 5–μm commercial Mg microparticles (FMW20, Tangshan Weihao Magnesium Powder Co.) as the core. The Mg microparticles were washed two times with acetone and dried under an N_2 current to remove impurities. Then, ~10 mg of Mg microparticles were dispersed onto glass slides, which were previously coated with 100 μl of 0.5% polyvinylpyrrolidone ethanolic solution (Spectrum Chemical). A coating of TiO_2 was deposited onto the Mg microparticles by atomic layer deposition at 100°C for 3000 cycles using a Beneq TFS 200 System, leaving a small opening at the contact point between the Mg particles and the glass slide. Last, the Mg micromotors were released by gentle scratching from the glass slide. For surface modification with a fluorescent dye, 0.5 mg of Mg micromotors were first mixed with 0.1% poly-L-lysine (Sigma-Aldrich) aqueous solution for 30 min. Then, 2 μg of 5/6-carboxyfluorescein succinimidyl ester (NHS-fluorescein; Thermo Fisher Scientific) was mixed with the motors in PBS buffer for 1 hour. The resulting fluorescein-labeled Mg micromotors were centrifuged at 3000*g* for 3 min, washed with ultrapure water, and dried for further use.

Preparation of fluorescent dye–labeled algae

Green algae were washed three times with ultrapure water to remove TAP medium and then suspended in HEPES buffer (Thermo Fisher Scientific). Then, 2 μg of NHS-fluorescein was added to 1 ml of algae at 2×10^6 per ml and incubated for 1 hour at room temperature. After dye conjugation, the modified algae were washed three times with TAP medium to remove free dye, and then they were suspended in TAP medium for further use. Near-infrared dye-labeled algae were prepared with a similar method by replacing NHS-fluorescein with NHS-Cy7 (Lumiprobe).

Synthesis of Dox-loaded polymeric NPs

Dox-loaded polymeric NPs were synthesized following a published method with slight modification (*49*). First, 50 μl of 25 mg/ml Dox-HCl (Sigma-Aldrich) solution was emulsified in 500 μl of a chloroform solution containing PLGA (50 mg/ml; 50:50, 0.66 dl/g; LACTEL Absorbable Polymers) using a Fisher Scientific FB120 ultrasonic probe sonicator operating at a power of 10 W. The process lasted for 2 min with alternating cycles of 2-s power on and 2-s power off in an ice bath. Then, the emulsion was transferred to 5 ml of tris-HCl (Teknova) aqueous solution and sonicated for another 2 min. The emulsion was stirred for 3 hours to completely remove the chloroform. The NPs were centrifuged at 16,100*g* for 5 min, washed three times with ultrapure water, and lyophilized for further use. NPs loaded with DiI (Thermo Fisher Scientific) were prepared using a similar procedure by replacing Dox with the dye.

Synthesis of cell membrane–coated NPs

RBC membrane–coated NPs were synthesized by a membrane cloaking technique (*40*). RBC membrane was mixed with PLGA cores at a 1:1 membrane protein to polymer weight ratio. The mixture was sonicated in a Fisher Scientific FS30D ultrasonic bath sonicator for 3 min. The NPs were isolated by centrifugation for 5 min at 16,100*g* and washed three times with ultrapure water. To characterize NP morphology, we deposited samples onto a carbon-coated 400-mesh copper grid and stained them with 1 weight % of uranyl acetate (Electron Microscopy Sciences), followed by imaging on a JEOL 1200 EX II TEM.

Preparation of algae-NP motors

To attach NPs onto algae, we washed 1×10^7 green algae three times with ultrapure water and treated them with 20 μM dibenzocyclooctyne-(polyethylene glycol)$_4$-*N*-hydroxysuccinimidyl ester (DBCO-PEG$_4$-NHS; Click Chemistry Tools) for 1 hour at room temperature. The NPs were incubated with 20 μM azide-PEG$_4$-NHS for 1 hour at room temperature. Both the algae and NPs were washed five times with ultrapure water to remove the unreacted NHS ester. Then, the modified algae and NPs were mixed together and vortexed for 3 hours to complete the click chemistry reaction. After conjugation, the resulting algae-NP motors were separated by centrifugation for 3 min at 500*g*, washed three times with TAP medium, and resuspended in TAP medium for further use. NP(Dox) conjugation onto the algae followed a similar method by replacing NPs with NP(Dox). To evaluate the NP(Dox) loading efficiency, we conjugated algae motors at 1×10^6/ml to NP(Dox) with Dox content at different concentrations (6.25, 12.5, 25, and 50 μg/ml). After fabrication of the algae-NP(Dox) motor, Dox content in unbound NP(Dox) was quantified by measuring the absorbance at 480 nm using a ultraviolet-visible spectrometer. The Dox loading amount on the algae motor was calculated by subtracting the unbound Dox from the Dox input.

Phototaxis of algae-NP motors

Phototaxis studies were conducted in three-dimensional printed microfluidic channels with a 5-mm by 4-mm by 2-mm chamber. Before testing, the channel was prefilled with 50 μl of TAP medium. Then, the algae-NP motors were added to one side of the channel, whereas the other side was illuminated using a light-emitting diode white light for 500 s. As a control, algae motors were added to one side without a light source on the other side. Time-lapse videos were recorded at 10 s per frame using an Invitrogen EVOS FL fluorescence microscope with a 2× objective.

Influence of Dox on algae viability

To evaluate the influence of free drug, we suspended algae motors at 1×10^6/ml into solutions containing different concentrations (0, 5, 10, and 25 μg/ml) of Dox. After 24 hours of incubation, each sample was collected, washed three times with ultrapure water to remove free drug, and resuspended into ultrapure water. Next, the samples were stained in 5 μM SYTOX fluorescent probe (Thermo Fisher Scientific) to measure algae viability. A similar method was used to test the viability of algae after conjugation of NP(Dox).

In vitro anticancer activity of algae-NP(Dox) motors

B16-F10 mouse melanoma cell lines (CRL-6475, American Type Culture Collection) were seeded into a 96-well plate at 5×10^4 per well and further incubated with free Dulbecco′s modified Eagle′s medium, free Dox, free algae, and algae-NP(Dox) motors for 24, 48, and 72 hours. All drug-containing wells used the same Dox concentration of 50 μg/ml. An MTS assay (Promega) was used to evaluate the cell viability per the manufacturer′s protocol.

Algae motility analysis

To evaluate their motion, we suspended unmodified algae motors, fluorescein-conjugated algae motors, and algae-NP motors in SIF (RICCA Chemical). Then, the algae were observed at 0 min, 5 min, 15 min, 30 min, 4 hours, and 12 hours at room temperature (22°C). In a separate experiment, algae were observed at 0 min, 5 min, 10 min, 15 min, 4 hours, and 12 hours at body temperature (37°C). For Mg micromotor motion analysis, the motors were uniformly dispersed on a glass slide, followed by addition of SIF solution. Motion was evaluated at the same time points as above, and SIF was continuously supplemented to prevent the motors from drying. To test the influence of NP(Dox) on motility, we measured the motion of algae-NP(Dox) motors in SIF. To evaluate the operation of algae motors in a mucus-rich environment, we analyzed their motion behavior in a simulated porcine small intestinal mucus containing mucin (20 mg/ml; Alfa Aesar) (*43*). Bright-field movies were captured by a Nikon Eclipse Ti-S/L100 inverted optical microscope coupled with different objectives (10× and 20×) and a Hamamatsu digital camera C11440. Meanwhile, fluorescent movies were captured using a Sony RX100 V camera on an Invitrogen EVOS FL fluorescence microscope with different objectives (20× and 40×) in two fluorescence channels, green fluorescent protein (GFP) and red fluorescent protein, corresponding to fluorescein and DiI. An NIS Element tracking module was used to measure the speed of the motors in SIF.

Characterization of algae-NP motors

To confirm NP binding on the surface of the algae motors, we labeled the RBC membrane on the NPs beforehand with DiO (Thermo Fisher Scientific). Fluorescence microscopy images were captured by using an Invitrogen EVOS FL microscope in two fluorescence channels, Cy5 and GFP, corresponding to the autofluorescence of the algae and DiO. To further confirm the structure of algae-NP motors, we performed SEM to visualize their morphology. The algae-NP motors were first fixed with a 2.5% glutaraldehyde solution (Sigma-Aldrich) overnight at 4°C and then washed three times with ultrapure water. The samples were sputtered with palladium for imaging on a Zeiss Sigma 500 SEM instrument using an acceleration voltage of 3 kV.

Fabrication of algae motor capsules

Mouse-specific size M gel capsules were supplied by Torpac. To perform the hydrophobic inner coating, we prepared 4% (w/w) of OTMS (Tokyo Chemical Industry) solution in pure ethanol and stirred it at room temperature for 2 hours. An insulin syringe was used to fill the capsule with ~4 μl of the OTMS solution, followed by a curing process at 120°C for 1 hour to completely evaporate the solvent. This process was repeated for up to 10 times to add more coating layers, and the capsules were stored at room temperature. For algae motor encapsulation, 4 μl of algae at a concentration of 2.5×10^5 per μl in TAP medium was slowly injected into the capsule using a primed syringe pump. After algae encapsulation, the commercial enteric coating polymer Eudragit L100-55 (Evonik Industries) was selected to coat the capsule for protection from gastric acid. First, the enteric coating polymer was dissolved at 7% (w/v) in ethanol solution by stirring at room temperature overnight. The capsules were then immersed into the enteric coating solution with a dip-coating approach, followed by solvent evaporation for a total of three times. After enteric coating, the capsules were stored at room temperature. To evaluate the release of algae motors from the capsule formulation, we immersed the loaded capsules either into SGF at pH 1.5 comprising 0.2% (w/w) sodium chloride and 0.31% (w/w) hydrochloric acid or into SIF at pH 6.8 containing 0.68% (w/w) potassium dihydrogen phosphate and 0.15% (w/w) sodium hydroxide under stirring at 700 rpm. For biodistribution studies, the static algae control (1×10^6), fluorescein-conjugated algae (2×10^6), fluorescein-labeled Mg motors (0.5 mg), and algae-NP(Dox) motors (5 μg of Dox) were encapsulated by a similar process. To generate the static algae control, we rapidly treated live algae with 0.5 M acetic acid to remove their flagella. To quantify the autofluorescence of algae motor and static algae samples, we used a Tecan Infinite M200 plate reader.

Animal care

Mice were housed in an animal facility at the University of California San Diego (UCSD) under federal, state, local, and National Institutes of Health (NIH) guidelines. Six-week-old CD-1 male mice were purchased from Charles River Labs. Mice were maintained in standard housing with cycles of 12-hour light and 12-hour dark, ambient temperature, and normal humidity. All animal experiments were performed in accordance with NIH guidelines and approved by the Institutional Animal Care and Use Committee of UCSD.

Pharmacokinetics and biodistribution studies

To characterize the biodistribution of algae motors, we fed male CD-1 mice an alfalfa-free diet (LabDiet, St. Louis, MO, USA) starting 1 week before the experiments. To compare the biodistribution between fluorescein-labeled algae motors (2×10^6) and Mg-based motors (0.5 mg), we administered mice with the corresponding capsules containing the motors labeled with equal amounts of dye. To evaluate the influence of active propulsion and capsule protection, we administered mice with encapsulated active algae (1×10^6), encapsulated static algae (1×10^6), unencapsulated active algae (1×10^6), or PBS by oral gavage. The mice were euthanized at 5 hours after administration. The entire GI tracts were then collected, rinsed with PBS, and imaged using a Xenogen IVIS 200 system. For quantitative fluorescent measurements, the collected tissues were weighed and then homogenized in PBS. The fluorescent signals were quantified using a Tecan Infinite M200 plate reader. To evaluate drug retention, we administered male CD-1 mice with algae-NP(Dox) motor capsules (5 μg of Dox), NP(Dox) capsules (5 μg of Dox), and PBS via oral gavage. At 3, 6, and 9 hours after oral administration, the GI tracts were then collected, weighed, and then homogenized in PBS. The amount of Dox was quantified using a Tecan Infinite M200 plate reader based on absorbance readings at 480 nm.

In vivo safety studies

Mice were euthanized at 24 hours after oral administration of TAP medium or encapsulated algae motors (1×10^6). For the comprehensive metabolic panel, aliquots of blood were allowed to coagulate, and the serum was collected by centrifugation. To obtain blood cell counts, we collected whole blood into potassium EDTA collection tubes (Sarstedt). For long-term safety, mice were administered algae motors in a capsule on days 0, 2, 4, and 6, and they were euthanized for analysis on day 7. Laboratory tests were performed by the UCSD Animal Care Program Diagnostic Services Laboratory. To perform the histological analysis, we sectioned different parts of the GI tract and major organs and stained them with H&E (Leica Biosystems), followed by imaging using a Hamamatsu Nanozoomer 2.0-HT slide scanning system.

Statistical analysis

All experiments were repeated as independent experiments several times, as shown by the figure captions. The results are reported as means ± SD. A two-tailed, Student's *t* test was used for testing the significance between two groups. A one-way analysis of variance (ANOVA) with Dunnett's test was performed to test the significance for multiple comparisons. Statistical significance is indicated as $^{*}P < 0.05$, $^{**}P < 0.01$, $^{***}P < 0.001$, and $^{****}P < 0.0001$. No data were excluded from the analysis. Samples were randomly allocated to different experimental groups. Organisms were cultured and maintained in the same environment and randomly allocated to each group. Investigators were not blinded during data collection and analysis.

Supplementary Materials

This PDF file includes:
Figs. S1 to S12

Other Supplementary Material for this manuscript includes the following:
Movies S1 to S10
MDAR Reproducibility Checklist

REFERENCES AND NOTES

1 J. Li, B. E.-F. de Ávila, W. Gao, L. Zhang, J. Wang, Micro/nanorobots for biomedicine: Delivery, surgery, sensing, and detoxification. *Sci. Robot.* **2**, eaam6431 (2017).

2 S. Hua, Advances in oral drug delivery for regional targeting in the gastrointestinal tract - influence of physiological, pathophysiological and pharmaceutical factors. *Front. Pharmacol.* **11**, 524 (2020).

3 L. M. Ensign, R. Cone, J. Hanes, Oral drug delivery with polymeric nanoparticles: The gastrointestinal mucus barriers. *Adv. Drug Deliv. Rev.* **64**, 557–570 (2012).

4 A. Abramson, M. R. Frederiksen, A. Vegge, B. Jensen, M. Poulsen, B. Mouridsen, M. O. Jespersen, R. K. Kirk, J. Windum, F. Hubálek, J. J. Water, J. Fels, S. B. Gunnarsson, A. Bohr, E. M. Straarup, M. W. Hvitfeld Ley, X. Lu, J. Wainer, J. Collins, S. Tamang, K. Ishida, A. Hayward, P. Herskind, S. T. Buckley, N. Roxhed, R. Langer, U. Rahbek, G. Traverso, Oral delivery of systemic monoclonal antibodies, peptides and small molecules using gastric auto-injectors. *Nat. Biotechnol.* **40**, 103–109 (2022).

5 A. Abramson, E. Caffarel-Salvador, V. Soares, D. Minahan, R. Y. Tian, X. Lu, D. Dellal, Y. Gao, S. Kim, J. Wainer, J. Collins, S. Tamang, A. Hayward, T. Yoshitake, H.-C. Lee, J. Fujimoto, J. Fels, M. R. Frederiksen, U. Rahbek, N. Roxhed, R. Langer, G. Traverso, A luminal unfolding microneedle injector for oral delivery of macromolecules. *Nat. Med.* **25**, 1512–1518 (2019).

6 J. Wu, H. Yuk, T. L. Sarrafian, C. F. Guo, L. G. Griffiths, C. S. Nabzdyk, X. Zhao, An off-the-shelf bioadhesive patch for sutureless repair of gastrointestinal defects. *Sci. Transl. Med.* **14**, eabh2857 (2022).

7 X. Liu, C. Steiger, S. Lin, G. A. Parada, J. Liu, H. F. Chan, H. Yuk, N. V. Phan, J. Collins, S. Tamang, G. Traverso, X. Zhao, Ingestible hydrogel device. *Nat. Commun.* **10**, 493 (2019).

8 N. G. Lamson, A. Berger, K. C. Fein, K. A. Whitehead, Anionic nanoparticles enable the oral delivery of proteins by enhancing intestinal permeability. *Nat. Biomed. Eng.* **4**, 84–96 (2020).

9 P. Angsantikul, K. Peng, A. M. Curreri, Y. Chua, K. Z. Chen, J. Ehondor, S. Mitraotri, Ionic liquids and deep eutectic solvents for enhanced delivery of antibodies in the gastrointestinal tract. *Adv. Funct. Mater.* **31**, 2002912 (2020).

10 A. Ghosh, L. Li, R. P. Dash, N. Gupta, J. Lam, Q. Jin, V. Akshintala, G. Pahapale, W. Liu, A. Sarkar, R. Rais, D. H. Gracias, F. M. Selaru, Gastrointestinal-resident, shape-changing microdevices extend drug release in vivo. *Sci. Adv.* **6**, eabb4133 (2020).

11 C. Gao, Y. Wang, Z. Ye, Z. Lin, X. Ma, Q. He, Biomedical micro−/nanomotors: From overcoming biological barriers to in vivo imaging. *Adv. Mater.* **33**, 2000512 (2020).

12 C. K. Schmidt, M. Medina-Sánchez, R. J. Edmondson, O. G. Schmidt, Engineering microrobots for targeted cancer therapies from a medical perspective. *Nat. Commun.* **11**, 5618 (2020).

13 Z. Wu, Y. Chen, D. Mukasa, O. S. Pak, W. Gao, Medical micro/nanorobots in complex media. *Chem. Soc. Rev.* **49**, 8088–8112 (2020).

14 B. Wang, K. Kostarelos, B. J. Nelson, L. Zhang, Trends in micro−/nanorobotics: Materials development, actuation, localization, and system integration for biomedical applications. *Adv. Mater.* **33**, 2002047 (2020).

15 B. Wang, K. F. Chan, K. Yuan, Q. Wang, X. Xia, L. Yang, H. Ko, Y.-X. J. Wang, J. J. Y. Sung, P. W. Y. Chiu, L. Zhang, Endoscopy-assisted magnetic navigation of biohybrid soft microrobots with rapid endoluminal delivery and imaging. *Sci. Robot.* **6**, eabd2813 (2021).

16 H. Zhang, Z. Li, C. Gao, X. Fan, Y. Pang, T. Li, Z. Wu, H. Xie, Q. He, Dual-responsive biohybrid neutrobots for active target delivery. *Sci. Robot.* **6**, eaaz9519 (2021).

17 A. C. Hortelao, C. Simó, M. Guix, S. Guallar-Garrido, E. Julián, D. Vilela, L. Rejc, P. Ramos-Cabrer, U. Cossío, V. Gómez-Vallejo, T. Patiño, J. Llop, S. Sánchez, Swarming behavior and in vivo monitoring of enzymatic nanomotors within the bladder. *Sci. Robot.* **6**, eabd2823 (2021).

18 Z. Wu, J. Troll, H.-H. Jeong, Q. Wei, M. Stang, F. Ziemssen, Z. Wang, M. Dong, S. Schnichels, T. Qiu, P. Fischer, A swarm of slippery micropropellers penetrates the vitreous body of the eye. *Sci. Adv.* **4**, eaat4388 (2018).

19 B. E.-F. de Ávila, P. Angsantikul, J. Li, M. A. Lopez-Ramirez, D. E. Ramírez-Herrera, S. Thamphiwatana, C. Chen, J. Delezuk, R. Samakapiruk, V. Ramez, M. Obonyo, L. Zhang, J. Wang, Micromotor-enabled active drug delivery for in vivo treatment of stomach infection. *Nat. Commun.* **8**, 272 (2017).

20 X. Wei, M. Beltrán-Gastélum, E. Karshalev, B. Esteban-Fernández de Ávila, J. Zhou, D. Ran, P. Angsantikul, R. H. Fang, J. Wang, L. Zhang, Biomimetic micromotor enables active delivery of antigens for oral vaccination. *Nano Lett.* **19**, 1914–1921 (2019).

21 L. Cai, C. Zhao, H. Chen, L. Fan, Y. Zhao, X. Qian, R. Chai, Suction-cup-inspired adhesive micromotors for drug delivery. *Adv. Sci.* **9**, 2103384 (2021).

22 E. Karshalev, Y. Zhang, B. Esteban-Fernández de Ávila, M. Beltrán-Gastélum, Y. Chen, R. Mundaca-Uribe, F. Zhang, B. Nguyen, Y. Tong, R. H. Fang, L. Zhang, J. Wang, Micromotors for active delivery of minerals toward the treatment of iron deficiency anemia. *Nano Lett.* **19**, 7816–7826 (2019).

23 J. Wang, *Nanomachines: Fundamentals and Applications* (John Wiley & Sons, 2013).

24 Z. Hosseinidoust, B. Mostaghaci, O. Yasa, B.-W. Park, A. V. Singh, M. Sitti, Bioengineered and biohybrid bacteria-based systems for drug delivery. *Adv. Drug Deliv. Rev.* **106**, 27–44 (2016).

25 L. Ricotti, B. Trimmer, A. W. Feinberg, R. Raman, K. K. Parker, R. Bashir, M. Sitti, S. Martel, P. Dario, A. Menciassi, Biohybrid actuators for robotics: A review of devices actuated by living cells. *Sci. Robot.* **2**, eaaq0495 (2017).

26 V. Magdanz, S. Sanchez, O. G. Schmidt, Development of a sperm-flagella driven micro-bio-robot. *Adv. Mater.* **25**, 6581–6588 (2013).

27 F. Zhang, Z. Li, L. Yin, Q. Zhang, N. Askarinam, R. Mundaca-Uribe, F. Tehrani, E. Karshalev, W. Gao, L. Zhang, J. Wang, ACE2 receptor-modified algae-based microrobot for removal of SARS-CoV-2 in wastewater. *J. Am. Chem. Soc.* **143**, 12194–12201 (2021).

28 O. Felfoul, M. Mohammadi, S. Taherkhani, D. De Lanauze, Y. Z. Xu, D. Loghin, S. Essa, S. Jancik, D. Houle, M. Lafleur, L. Gaboury, M. Tabrizian, N. Kaou, M. Atkin, T. Vuong, G. Batist, N. Beauchemin, D. Radzioch, S. Martel, Magneto-aerotactic bacteria deliver drug-containing nanoliposomes to tumour hypoxic regions. *Nat. Nanotechnol.* **11**, 941–947 (2016).

29 H. Xu, M. Medina-Sánchez, V. Magdanz, L. Schwarz, F. Hebenstreit, O. G. Schmidt, Sperm-hybrid micromotor for targeted drug delivery. *ACS Nano* **12**, 327–337 (2018).

30 M. Medina-Sánchez, L. Schwarz, A. K. Meyer, F. Hebenstreit, O. G. Schmidt, Cellular cargo delivery: Toward assisted fertilization by sperm-carrying micromotors. *Nano Lett.* **16**, 555–561 (2015).

31 S. Xie, L. Zhao, X. Song, M. Tang, C. Mo, X. Li, Doxorubicin-conjugated Escherichia coli Nissle 1917 swimmers to achieve tumor targeting and responsive drug release. *J. Control. Release* **268**, 390–399 (2017).

32 O. Yasa, P. Erkoc, Y. Alapan, M. Sitti, Microalga-powered microswimmers toward active cargo delivery. *Adv. Mater.* **30**, 1804130 (2018).

33 M. B. Akolpoglu, N. O. Dogan, U. Bozuyuk, H. Ceylan, S. Kizilel, M. Sitti, High-yield production of biohybrid microalgae for on-demand cargo delivery. *Adv. Sci.* **7**, 2001256 (2020).

34 I. P. Kerschgens, K. Gademann, Antibiotic algae by chemical surface engineering. *Chembiochem* **19**, 439–443 (2018).

35 T. J. Böddeker, S. Karpitschka, C. T. Kreis, Q. Magdelaine, O. Bäumchen, Dynamic force measurements on swimming *Chlamydomonas* cells using micropipette force sensors. *J. R. Soc. Interface* **17**, 20190580 (2020).

36 D. B. Weibel, P. Garstecki, D. Ryan, W. R. DiLuzio, M. Mayer, J. E. Seto, G. M. Whitesides, Microoxen: Microorganisms to move microscale loads. *Proc. Natl. Acad. Sci. U.S.A.* **102**, 11963–11967 (2005).

37 B. P.-H. Huang, *Chlamydomonas reinhardtii*: A model system for the genetic analysis of flagellar structure and motility. *Int. Rev. Cytol.* **99**, 181–215 (1986).

38 K. Y. Wan, R. E. Goldstein, Coordinated beating of algal flagella is mediated by basal coupling. *Proc. Natl. Acad. Sci. U.S.A.* **113**, E2784–E2793 (2016).

39 S. Kalkhof, A. Sinz, Chances and pitfalls of chemical cross-linking with amine-reactive N-hydroxysuccinimide esters. *Anal. Bioanal. Chem.* **392**, 305–312 (2008).

40 C.-M. J. Hu, L. Zhang, S. Aryal, C. Cheung, R. H. Fang, L. Zhang, Erythrocyte membrane-camouflaged polymeric nanoparticles as a biomimetic delivery platform. *Proc. Natl. Acad. Sci. U.S.A.* **108**, 10980–10985 (2011).

41 J. D. Cox, M. S. Curry, S. K. Skirboll, P. L. Gourley, D. Y. Sasaki, Surface passivation of a microfluidic device to glial cell adhesion: A comparison of hydrophobic and hydrophilic SAM coatings. *Biomaterials* **23**, 929–935 (2002).

42 J. Li, S. Thamphiwatana, W. Liu, B. Esteban-Fernández de Ávila, P. Angsantikul, E. Sandraz, J. Wang, T. Xu, F. Soto, V. Ramez, X. Wang, W. Gao, L. Zhang, J. Wang, Enteric micromotor can selectively position and spontaneously propel in the gastrointestinal tract. *ACS Nano* **10**, 9536–9542 (2016).

43 M. Boegh, H. M. Nielsen, Mucus as a barrier to drug delivery – Understanding and mimicking the barrier properties. *Basic Clin. Pharmacol. Toxicol.* **116**, 179–186 (2015).

44 F. Zhang, R. Mundaca-Uribe, H. Gong, B. Esteban-Fernández de Ávila, M. Beltrán-Gastélum, E. Karshalev, A. Nourhani, Y. Tong, B. Nguyen, M. Gallot, Y. Zhang, L. Zhang, J. Wang, A macrophage–magnesium hybrid biomotor: Fabrication and characterization. *Adv. Mater.* **31**, 1901828 (2019).

45 D. Zhong, D. Zhang, W. Chen, J. He, C. Ren, X. Zhang, N. Kong, W. Tao, M. Zhou, Orally deliverable strategy based on microalgal biomass for intestinal disease treatment. *Sci. Adv.* **7**, eabi9265 (2021).

46 Y. Inoue, K. Izawa, S. Kiryu, A. Tojo, K. Ohtomo, Diet and abdominal autofluorescence detected by in vivo fluorescence imaging of living mice. *Mol. Imaging* **7**, 21–27 (2008).

47 O. Tacar, P. Sriamornsak, C. R. Dass, Doxorubicin: An update on anticancer molecular action, toxicity and novel drug delivery systems. *J. Pharm. Pharmacol.* **65**, 157–170 (2013).

48 R. H. Fang, A. V. Kroll, W. Gao, L. Zhang, Cell membrane coating nanotechnology. *Adv. Mater.* **30**, 1706759 (2018).

49 N. Yang, Y. Ding, Y. Zhang, B. Wang, X. Zhao, K. Cheng, Y. Huang, M. Taleb, J. Zhao, W.-F. Dong, Surface functionalization of polymeric nanoparticles with umbilical cord-derived mesenchymal stem cell membrane for tumor-targeted therapy. *ACS Appl. Mater. Interfaces* **10**, 22963–22973 (2018).

50 X. Yan, Q. Zhou, M. Vincent, Y. Deng, J. Yu, J. Xu, T. Xu, T. Tang, L. Bian, Y.-X. J. Wang, K. Kostarelos, L. Zhang, Multifunctional biohybrid magnetite microrobots for imaging-guided therapy. *Sci. Robot.* **2**, eaaq1155 (2017).

51 H.-M. D. Wang, X.-C. Li, D.-J. Lee, J.-S. Chang, Potential biomedical applications of marine algae. *Bioresour. Technol.* **244**, 1407–1415 (2017).

52 Y. Qiao, F. Yang, T. Xie, Z. Du, D. Zhong, Y. Qi, Y. Li, W. Li, Z. Lu, J. Rao, Y. Sun, M. Zhou, Engineered algae: A novel oxygen-generating system for effective treatment of hypoxic cancer. *Sci. Adv.* **6**, eaba5996 (2020).

53 Z. Wu, L. Li, Y. Yang, P. Hu, Y. Li, S.-Y. Yang, L. V. Wang, W. Gao, A microrobotic system guided by photoacoustic computed tomography for targeted navigation in intestines in vivo. *Sci. Robot.* **4**, eaax0613 (2019).

54 B. W. Jester, H. Zhao, M. Gewe, T. Adame, L. Perruzza, D. T. Bolick, J. Agosti, N. Khuong, R. Kuestner, C. Gamble, K. Cruickshank, J. Ferrara, R. Lim, T. Paddock, C. Brady, S. Ertel, M. Zhang, A. Pollock, J. Lee, J. Xiong, M. Tasch, T. Saveria, D. Doughty, J. Marshall, D. Carrieri, L. Goetsch, J. Dang, N. Sanjaya, D. Fletcher, A. Martinez, B. Kadis, K. Sigmar, E. Afreen, T. Nguyen, A. Randolph, A. Taber, A. Krzeszowski, B. Robinett, D. B. Volkin, F. Grassi, R. Guerrant, R. Takeuchi, B. Finrow, C. Behnke, J. Roberts, Development of spirulina for the manufacture and oral delivery of protein therapeutics. *Nat. Biotechnol.* **40**, 974 (2022).

55 M. A. Scranton, J. T. Ostrand, F. J. Fields, S. P. Mayfield, Chlamydomonas as a model for biofuels and bio-products production. *Plant J.* **82**, 523–531 (2015).

Acknowledgments

Funding: This work is supported by the NIH under award numbers R01CA200574 and R21AI159492 and the Defense Threat Reduction Agency Joint Science and Technology Office for Chemical and Biological Defense under grant number HDTRA1-18-1-0014. **Author contributions:** All authors contributed to the writing of the manuscript. All authors have given approval to the final version of the manuscript. **Competing interests:** The authors declare that they have no competing interests. **Data and materials availability:** All data needed to evaluate the conclusions in the paper are present in the paper or the Supplementary Materials.

Submitted 2 February 2022
Accepted 31 August 2022
Published 28 September 2022
10.1126/scirobotics.abo4160